

However, the factorial ANOVA has shown that the scan length was not of critical importance in determining the I_T values in the human brain regions: the 6-h scan time seems to have allowed more sensitive evaluation of the thalamic region. That is because the kinetics of ^{123}I -5IA in the human brain have some peculiarities for the thalamus (later peak of radioactivity in the brain around 110 min), making the longer scans more suitable for estimating the nAChRs in the thalamic regions.

Based on these results, another group of subjects (group 2) was included and scanned using a short scan time (90 min) (Table 4). To verify the reproducibility of measurement using a short scan time, subjects of around 20 y old were grouped (subjects 7–13). The I_T values were calculated and their results were compared with those I_T values calculated from the first group (using a 90-min time interval) for the same age (subjects 1–6). No significant difference was observed between them, confirming the reproducibility of the measurement with a short scan time.

Once the data for all volunteers (first group analyzed in a 90-min time interval and second group) were assembled in a single group (Table 4), the distribution of I_T values showed a pattern similar to that described for the 6-h scan time, with the highest I_T values for the thalamus (ANOVA, $P < 0.01$). Some studies have mentioned aged-related changes in the nicotinic neuroreceptors in the human brain (2,7,10), but our study did not observe statistically significant values. The inability to observe age-related changes in this study is probably due to the small number of subjects from different age groups. Further studies might be necessary to elucidate the age-related change in human nAChRs.

CONCLUSION

We have described a novel method for the quantitative analysis of nAChRs in the human brain using ^{123}I -5IA. A 2-compartment model analysis (2-parameter configuration) was chosen to fit the present data, and results were relatively stable across all regions. Three different levels of density of nAChRs in the human brain (expressed as I_T) were identified. The I_T values showed the highest density of nAChRs to be in the thalamus; moderate densities were found in the brain stem, basal ganglia, and cerebellum, and low densities were found in the frontal, parietal, temporal, and occipital cortices. Good agreement was observed between I_T values and autoradiographic studies done in vitro for nAChR density in human brain. A high correlation index was observed between distribution volumes from the compartmental model and graphical analyses. Our results indicate that ^{123}I -5IA SPECT is suitable for the quantification of nAChRs in the human brain.

ACKNOWLEDGMENTS

The authors thank Dr. Sadahiko Nishizawa, Hamamatsu Medical Photonics Foundation, for valuable comments, and Dr. Mahbubur Rahman, Department of Epidemiological and

Clinical Research Information Management, Kyoto University, for advice regarding the statistical analysis. This work was supported in part by a grant from the Research for the Future Program of the Japan Society for the Promotion of Science (JSPS-RFTF97K00201), Grants-in-Aid for Scientific Research from the Ministry of Education, Science and Technology of Japan, a research grant for Longevity Sciences from the Ministry of Health and Welfare, and a grant from the Smoking Research Foundation. The authors thank Nihon Medi-Physics Co. Ltd., Japan, for providing sodium ^{123}I -iodide.

REFERENCES

- Lindstrom J, Anand R, Peng X, Gerzanich V, Wang F, Li Y. Neuronal nicotinic receptor subtypes. *Ann NY Acad Sci*. 1995;757:100–116.
- Paterson D, Nordberg A. Neuronal nicotinic receptors in the human brain. *Prog Neurobiol*. 2000;61:75–111.
- Whiting P, Esch F, Shimasaki S, Lindstrom J. Neuronal nicotinic acetylcholine receptor beta-subunit is coded for by the cDNA clone alpha 4. *FEBS Lett*. 1987;219:459–463.
- Flores CM, Rogers SW, Pabreza LA, Wolfe EB, Kellar KJ. A subtype of nicotinic cholinergic receptor in rat brain is composed of alpha 4 and beta 2 subunits and is up-regulated by chronic nicotine treatment. *Mol Pharmacol*. 1992;41:31–37.
- Zoli M, Lena C, Picciotto MR, Changeux JP. Identification of four classes of brain nicotinic receptors using beta2 mutant mice. *J Neurosci*. 1998;18:4461–4472.
- Changeux JP, Bertrand D, Corringer PJ, et al. Brain nicotinic receptors: structure and regulation, role in learning and reinforcement. *Brain Res Brain Res Rev*. 1998;26:198–216.
- Whitehouse PJ, Au KS. Cholinergic receptors in aging and Alzheimer's disease. *Prog Neuropsychopharmacol Biol Psychiatry*. 1986;10:665–676.
- Perry EK, Morris CM, Court JA, et al. Alteration in nicotine binding sites in Parkinson's disease, Lewy body dementia and Alzheimer's disease: possible index of early neuropathology. *Neuroscience*. 1995;64:385–395.
- Shiver W, Gillberg PG, Svensson AL, Nordberg A. Autoradiographic comparison of [^3H]-nicotine, [^3H]-cytisine and [^3H]-epibatidine binding in relation to vesicular acetylcholine transport sites in the temporal cortex in Alzheimer's disease. *Neuroscience*. 1999;94:685–696.
- Shimohama S, Taniguchi T, Fujivara M, Kameyama M. Changes in nicotinic and muscarinic cholinergic receptors in Alzheimer-type dementia. *J Neurochem*. 1986;46:288–293.
- Marks MJ, Romm E, Gaffney DK, Collins AC. Nicotine-induced tolerance and receptor changes in four mouse strains. *J Pharmacol Exp Ther*. 1986;237:809–819.
- Benwell ME, Balfour DJ, Anderson JM. Evidence that tobacco smoking increases the density of (+)-[^3H]nicotine binding sites in human brain. *J Neurochem*. 1988;50:1243–1247.
- Perry DC, Davila-Garcia MI, Stockmeier CA, Kellar KJ. Increased nicotinic receptors in brains from smokers: membrane binding and autoradiography studies. *J Pharmacol Exp Ther*. 1999;289:1545–1552.
- Ereese CR, Marks MJ, Logel J, et al. Effect of smoking history on [^3H]nicotine binding in human postmortem brain. *J Pharmacol Exp Ther*. 1997;282:7–13.
- Sullivan JP, Donnelly-Roberts D, Briggs CA, et al. A-85380 [3-(2S)-azetidyl-methoxy]pyridine] in vitro pharmacological properties of a novel, high affinity alpha 4 beta 2 nicotinic acetylcholine receptor ligand. *Neuropharmacology*. 1996;35:725–734.
- Koren AO, Horti AG, Mukhin AG, et al. 2-, 5-, and 6-Halo-3-(2S)-azetidyl-methoxy pyridines: synthesis, affinity for nicotinic acetylcholine receptors, and molecular modeling. *J Med Chem*. 1998;41:3690–3698.
- Mukhin AG, Gundusch D, Horti AG, et al. 5-Iodo-A-85380, an alpha4beta2 subtype-selective ligand for nicotinic acetylcholine receptors. *Mol Pharmacol*. 2000;57:642–649.
- Saji H, Ogawa M, Ueda M, et al. Evaluation of radioiodinated 5-iodo-3-(2S)-azetidylmethoxy pyridine as a ligand for SPECT investigations of brain nicotinic acetylcholine receptors. *Ann Nucl Med*. 2002;16:189–200.
- Chefer SI, Horti AG, Lee KS, et al. In vivo imaging of brain nicotinic acetylcholine receptors with 5-[^{123}I]iodo-A-85380 using single photon emission computed tomography. *Life Sci*. 1998;63:PL355–PL360.

- 20 Musachio JL, Scheffel U, Finley PA, et al. 5-[I-125]iodo-3-(2S)-azetidinylmethoxy pyridine, a radioiodinated analog of A-85380 for in vivo studies of central nicotinic acetylcholine receptors. *Life Sci*. 1998;62:PL351-PL357.
- 21 Musachio JL, Villemagne VL, Scheffel UA, et al. Synthesis of an I-123 analog of A-85380 and preliminary SPECT imaging of nicotinic receptors in baboon. *Nucl Med Biol*. 1999;26:201-207.
- 22 Fujita M, Tamagnan G, Zoghbi SS, et al. Measurement of $\alpha_3\beta_2$ nicotinic acetylcholine receptors with [¹²³I]5-I-A-85380 SPECT. *J Nucl Med*. 2000;41:1552-1560.
- 23 Fujita M, Seibyl JP, Vaupel B, et al. Whole-body biodistribution, radiation absorbed dose, and brain SPET imaging with [¹²³I]5-I-A-85380 in healthy human subjects. *Eur J Nucl Med*. 2002;29:183-190.
- 24 Vaupel DB, Tella SR, Huso DL, et al. Pharmacology, toxicology, and radiation dosimetry evaluation of [I-123]5-I-a-85380, a radioligand for in vivo imaging of cerebral neuronal nicotinic acetylcholine receptors in humans. *Drug Dev Res*. 2003;58:149-168.
- 25 Mintum MA, Raichle ME, Kilbourn MR, Wooten GF, Welch MJ. A quantitative model for the in vivo assessment of drug binding sites with positron emission tomography. *Ann Neurol*. 1984;15:217-227.
- 26 Logan J, Fowler JS, Volkow ND, et al. Graphical analysis of reversible radioligand binding from time-activity measurements applied to [¹⁴C-methyl]-(-)-cocaine PET studies in human subjects. *J Cereb Blood Flow Metab*. 1990;10:740-747.
- 27 Ding Y, Liu N, Wang T, et al. Synthesis and evaluation of 6-[¹⁸F]fluoro-3-(2S)-azetidinylmethoxy pyridine as a PET tracer for nicotinic acetylcholine receptors. *Nucl Med Biol*. 2000;27:381-389.
- 28 Kimes AS, Horti AG, London ED, et al. 2-[¹⁸F]F-A-85380 PET imaging of brain nicotinic acetylcholine receptors and whole body distribution in humans. *FASEB J*. 2003;17:1331-1333.
- 29 Marutle A, Warpmann U, Bogdanovic N, Nordberg A. Regional distribution of subtypes of nicotinic receptors in human brain and effect of aging studied by (+)-[³H]epibatidine. *Brain Res*. 1998;801:143-149.
- 30 Niao Y, Meyer EL, Thompson JM, Surin A, Wroblewski J, Kellar KJ. Rat $\alpha_3\beta_4$ subtype of neuronal nicotinic acetylcholine receptor stably expressed in a transfected cell line: pharmacology of ligand binding and function. *Mol Pharmacol*. 1998;54:322-333.
- 31 Kulak JM, Sun J, Musachio JL, McIntosh JM, Quirk M. 5-Iodo-A-85380 binds to α -conotoxin MII-sensitive nicotinic acetylcholine receptors (nAChRs) as well as $\alpha_4\beta_2^*$ subtypes. *J Neurochem*. 2002;81:403-406.
- 32 Carson RE. Mathematical modeling and compartmental analysis. In: Harbert J, Eckelman WC, Neumann R, eds. *Nuclear Medicine: Diagnosis and Therapy*. New York, NY: Thieme Medical; 1996:167-194.

5-¹²³I]Iodo-A-85380: assessment of pharmacological safety, radiation dosimetry and SPECT imaging of brain nicotinic receptors in healthy human subjects

Masashi UEDA,* Yasuhiko IIDA,* Takahiro MUKAI,** Marcelo MAMEDE,** Koichi ISHIZU,**
Mikako OGAWA,*** Yasuhiro MAGATA,*** Junji KONISHI** and Hideo SAJI*

*Department of Patho-Functional Bioanalysis, Graduate School of Pharmaceutical Sciences, Kyoto University

**Department of Nuclear Medicine and Diagnostic Imaging, Graduate School of Medicine, Kyoto University

***Laboratory of Genome-Bio Photonics, Photon Medical Research Center, Hamamatsu University School of Medicine

Recently, 5-¹²³I]iodo-3-(2(*S*)-azetidylmethoxy)pyridine (¹²³I]5IA) was developed as a ligand for imaging the nicotinic acetylcholine receptor (nAChR) in human brain using single photon emission computed tomography (SPECT). In the present study, the toxicity and radiation absorbed dose of ¹²³I]5IA were investigated.

Behavior and physiological parameters were examined in mice and rats after administration of 5IA. There were no changes in these parameters in animals administered 1 μg/kg of 5IA or less, indicating that the no observed effect level (NOEL) of 5IA was 1 μg/kg. ¹²³I]5IA was then administered to healthy human subjects and serial whole-body images were acquired over 24 hr. Initially, high levels of radioactivity were observed in the liver and urinary bladder and moderate levels in the lungs, kidneys, and brain. Whole brain activity at 1 hr was 4.6 ± 0.4% of the injected dose and this value gradually decreased with time. The majority (~75%) of the radioactivity was excreted in urine within 24 hr, and less than 1% remained in all organs tested. The biological half-life of ¹²³I]5IA averaged 7.2 ± 4.0 hr. Based on the biodistribution data, radiation absorbed doses were estimated using MIRDose 3.1 software with the dynamic bladder model and the ICRP gastrointestinal (GI) tract model. Consequently, the effective dose equivalent was estimated to be 30 ± 1.4 μSv/MBq, which is an acceptable radiation burden. Having determined the safety of this compound, we performed SPECT imaging in a healthy human subject using 171 MBq of ¹²³I]5IA. SPECT images clearly revealed a cerebral distribution of radioactivity that was consistent with the known distribution of central nAChRs in humans. These results suggest that ¹²³I]5IA is a promising ligand for imaging nAChRs in humans, with an acceptable dosimetry and pharmacological safety at the dose required for adequate SPECT imaging.

Key words: 5-¹²³I]iodo-3-(2(*S*)-azetidylmethoxy)pyridine, pharmacological effects, radiation dosimetry, single photon emission computed tomography, nicotinic acetylcholine receptor

INTRODUCTION

NICOTINIC ACETYLCHOLINE RECEPTORS (nAChRs) are a family

Received December 13, 2003, revision accepted March 11, 2004.

For reprint contact: Hideo Saji, M.D., Department of Patho-Functional Bioanalysis, Graduate School of Pharmaceutical Sciences, Kyoto University, Yoshida Shimoadachi-cho, Sakyo-ku, Kyoto 606-8501, JAPAN.

E-mail: hsaji@pharm.kyoto-u.ac.jp

of ligand-gated ion channels that regulate neurotransmission in the central and peripheral nervous systems. These receptors are of great interest because they are implicated in various brain functions, such as cognition and memory,^{1,2} and in nicotine-induced neuroprotective³ and analgesic effects.⁴ In addition, changes in the density of nAChRs have been reported in various neurodegenerative disorders including Alzheimer's disease^{5,6} and Parkinson's disease.^{7,8} Thus, imaging of nAChRs in the brain with positron emission tomography (PET) or single photon emission computed tomography (SPECT) has been of

great interest for the evaluation of brain functions and the diagnosis of neurodegenerative disorders. The development of a radioligand suitable for this purpose has been desired.

Recently, 5-[¹²³I]iodo-3-(2(*S*)-azetidylmethoxy)pyridine (5IA), a derivative of A-85380 iodinated at the 5-position of the pyridine ring, was reported to be a promising ligand for imaging nAChRs because of its high uptake in the rodent and primate brain, a distribution consistent with the known density of nAChRs, and low non-specific binding.⁹⁻¹³ Thus, characterization of its pharmacological effects and information on its biodistribution and organ radiation burden in humans have been required for the clinical application of [¹²³I]5IA brain SPECT.

The Food and Drug Administration proposes that a test compound be administered to small numbers of animals to identify doses causing no adverse effect and does not recommend calculating lethality parameters using large numbers of animals.¹⁴ In the present study, we investigated changes in behavior in mice and in physiological parameters in rats after administration of 5IA to determine the NOEL of this ligand. Based on these results, the dose of [¹²³I]5IA was determined and then administered to healthy human volunteers to measure the whole-body distribution, to estimate the radiation absorbed doses, and to obtain SPECT images of [¹²³I]5IA in the human brain.

MATERIALS AND METHODS

Chemicals

5IA and 5-(tri-*n*-butylstannyl)-3-(1-*tert*-butoxycarbonyl)-2(*S*)-azetidylmethoxy)pyridine, the stannyl precursor of [¹²³I]5IA, were synthesized according to a previous report.¹³ No carrier-added sodium [¹²³I]iodine was supplied by Nihon Medi-Physics Co. Ltd. (Nishinomiya, Japan). All other chemicals used were of reagent grade.

Studies in animals

Male ICR mice and male Sprague-Dawley rats were supplied by Japan SLC Co. Ltd. (Hamamatsu, Japan). The animal experiments were conducted in accordance with our institutional guidelines and approved by the Kyoto University Animal Care Committee. 5IA was injected as a physiological saline solution.

Behavioral test

Male ICR mice weighing 28–32 g were separated into four groups (five per group) and injected intravenously with either vehicle or one of three doses of 5IA: 10 µg/kg = 27.5 nmol/kg, 1 µg/kg = 2.75 nmol/kg, or 0.1 µg/kg = 0.275 nmol/kg. For 60 min after the administration, the righting reflex, motor functions and spontaneous locomotion were observed. Mice were bred for another week after 5IA administration, and the sub-acute toxicity of 5IA was assessed by measuring their weights.

Changes in physiological parameters

Male Sprague-Dawley rats weighing 280–320 g were anesthetized with chloral hydrate (400 mg/kg intraperitoneal injection) and implanted with a catheter into the left femoral artery. The catheter was connected through a three-way stopcock to a pressure transducer (COBE, Cobe Laboratory Inc., USA) and a monitor (CM-861, Fukuda Denshi Co. Ltd., Tokyo, Japan) for measuring arterial blood pressure. Heart rate, respiratory rate, blood gases (PCO₂ and PO₂), and blood pH were also measured. Heart rate was measured using the same monitor. Respiratory rate was counted with the naked eye. Blood pH and blood gases were determined with a dedicated analyzer (M278 Blood Gas System, Ciba-Corning, Germany). Prior to the administration of 5IA, basal values of each parameter were obtained.

Rats were separated into four groups (four or five per group) and injected intravenously with vehicle or one of three doses of 5IA: 5 µg/kg = 13.8 nmol/kg, 2 µg/kg = 5.51 nmol/kg, or 1 µg/kg = 2.75 nmol/kg. Mean arterial blood pressure (MABP) and heart rate were monitored continuously up to 60 min after the administration of each drug. The respiratory rate was counted 1, 2, 3, 5, 15, 30, 45, and 60 min after the administration. Blood pH and blood gases were determined by withdrawing blood via the three-way stopcock at 5, 15, 30, 45, and 60 min. The body temperature of each rat was maintained at 37°C throughout the study.

Data were analyzed using a one-way analysis of variance (ANOVA) followed by Dunnett's test to compare the parameters after the drug administration to the baseline. Differences were considered significant when $p < 0.05$.

Studies in humans

These experiments were approved by the Institutional Review Board of Kyoto University Hospital.

Radiolabeling

Radiolabeling was performed according to a previous report¹³ with slight modifications. Briefly, reagents were added into a vial in the following order: no-carrier-added sodium [¹²³I]iodine (1110 MBq), 100 µg of stannyl precursor (10 µl of ethanolic solution), 160 µl of 1.5% acetic acid, 10 µl of 3 mol/l HCl, and 20 µl of 5% H₂O₂ solution as an oxidant. The mixture was stirred at 75°C for 15 min. Concentrated HCl was then added and the resulting solution stirred for 10 min at 75°C. The mixture was basified with sodium hydroxide, extracted with ethyl acetate, and purified by reverse-phase HPLC. After rotary evaporation of the eluent, the residue was formulated in 0.9% saline and filtered through a 0.2 µm filter into a sterile vial. Sterility was confirmed by lack of growth in tryptone soya broth/gelatin peptone. No endotoxin was detected by a limulus test based on the ability of endotoxin to induce coagulation of the amoebocyte lysate of the horseshoe crab, *Limulus polyphemus*. Radiochemical yield was more

than 40% and radiochemical purity was greater than 98%. The specific activity determined from the UV absorbance at 254 nm was more than 169 GBq/ μ mol (the limit of detection with this method).

Subjects

Three healthy males were recruited for the whole-body scan (age: 19, 20, 67 years) and another healthy male was recruited for the brain SPECT (age: 20 years). All volunteers were nonsmokers. Before the imaging, written informed consent was obtained from each participant.

Whole-body image acquisition

Volunteers were positioned supine with their arms alongside their body. Whole-body images were acquired using a dual-headed gamma camera (RC-2500IV, Hitachi Medical Co., Tokyo, Japan). In this system, a low-energy high-resolution collimator was used, and the energy peak was centered at 159 keV with a 20% energy window.

Whole-body planar images were acquired 0.5, 1, 2, 5 and 24 hr after the injection of 100 MBq of [¹²³I]5IA. Acquisition was performed simultaneously in anterior and posterior positions. The scan speed was 15 cm/min and Matrix size was 256 × 1024 pixels.

Urine collection

Urine was collected up to 24 hr after injection. The volunteers were briefed to collect their urine and to record the volume and time of voidance. From each urine sample, three aliquots were measured in an automatic gamma counter (Aloka Co. Ltd., Tokyo, Japan). Measurements of radioactivity were corrected for physical decay and multiplied by the urine volume at each voidance. The total amount of radioactivity was expressed as a percentage of the injected radioactivity (% ID) of [¹²³I]5IA.

Image analysis

The quantification of uptake after injection of [¹²³I]5IA was performed using a region of interest (ROI) method. ROIs were drawn over the whole-body or various organs (brain, thyroid, lungs, heart, liver, spleen, abdomen, and left kidney) using HARP-III (Hitachi Medical Co., Tokyo, Japan). All ROIs were drawn by the same operator to minimize variability in region definition. The activity in

the abdomen meant the gastrointestinal activity excluding liver, spleen, kidneys, and urinary bladder. The activity in kidneys was determined by doubling that in the left kidney, i.e., the activity in the right kidney was taken to be the same as that in the left. This was done to avoid overestimating the activity in the right kidney due to overlap with the liver. Almost all ROIs (except for the thyroid, which was drawn on the latest image) were drawn on the earliest images, and the shapes and sizes were kept constant in all subsequent images. ROIs drawn on the off-body region beside the volunteer's head were used as the instrumental background. After subtracting the instrumental background activity from the organ activity (as counts/pixel), the geometric mean of the anterior and posterior counts for the whole-body or each organ was calculated. The whole-body geometric mean count of the first scan was taken as the injected radioactivity, because the first images were acquired before excretion. The activity of the whole-body or each organ was calculated with the following equation: (geometric mean counts in whole-body or organ at each time point)/(geometric mean counts in first whole-body) × 100, and expressed as % ID.

Estimating radiation absorbed dose

For each individual, non-decay-corrected time-activity curves were generated for the brain, thyroid, lungs, heart, liver, spleen, and kidney. The terminal elimination phase

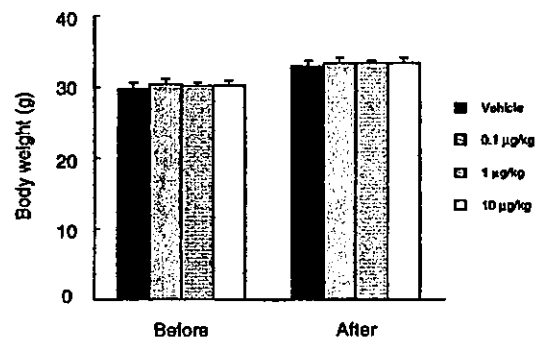


Fig. 1 Changes in body weight after administration of 5IA or vehicle. Mice were weighed before (Before) and 7 days after administration (After). No significant difference was observed between vehicle and 5IA-treated groups at either time point.

Table 1 Changes in behaviors after administration of 5IA

	Righting reflex		Grooming		Spontaneous locomotion	
	0–30 min	30–60 min	0–30 min	30–60 min	0–30 min	30–60 min
Vehicle	±	±	±	±	±	±
0.1 µg/kg	±	±	±	±	±	±
1 µg/kg	±	±	±	±	±	±
10 µg/kg	±	±	↓ (2)	±	↓ (5)	±

±: No change, ↓: Decrease

The number in parentheses represents the number of mice exhibiting the abnormal behavior. (5 mice in each group.)

of the curves was extrapolated to infinity. Organ residence times were determined by calculating the area under the extrapolated time-activity curves with the trapezoidal method using WinNonlin version 1.5 software. The residence time of urinary bladder was calculated by applying the dynamic bladder model,¹⁵ with a voiding interval of 4.8 hr (representing a rate of 5 times a day, typical of a

normal adult). Residence times of GI tracts were calculated by applying the ICRP 30 GI tract model,¹⁶ assuming that an activity passed through various segments of the GI tract at standard rates. Then using these residence times, organ absorbed doses and effective dose were estimated with the MIRDOSE 3.1 software package.¹⁷

Table 2 Effects of 5IA on respiratory rate (breaths/min)

	Baseline	1 min	2 min	3 min	5 min	15 min	30 min	45 min	60 min
Vehicle	104 ± 14	105 ± 20	108 ± 20	107 ± 16	113 ± 17	116 ± 19	118 ± 14	116 ± 9	111 ± 8
1 µg/kg	106 ± 16	113 ± 23	113 ± 17	114 ± 15	111 ± 14	114 ± 18	121 ± 21	119 ± 20	110 ± 18
2 µg/kg	111 ± 7	119 ± 16	117 ± 20	114 ± 30	116 ± 15	131 ± 15	125 ± 14	124 ± 14	120 ± 9
5 µg/kg	111 ± 4	162 ± 12#	150 ± 13#	144 ± 20#	141 ± 16#	138 ± 16#	138 ± 17#	128 ± 6*	126 ± 10

Values are mean ± s.d.

#p < 0.01, *p < 0.05 vs. Baseline.

Table 3 Effects of 5IA on heart rate (beats/min)

	Baseline	1 min	2 min	3 min	5 min	15 min	30 min	45 min	60 min
Vehicle	236 ± 16	227 ± 20	225 ± 16	236 ± 30	225 ± 21	221 ± 20	225 ± 17	224 ± 15	233 ± 26
1 µg/kg	230 ± 24	245 ± 17	242 ± 6	236 ± 15	243 ± 8	227 ± 6	234 ± 13	237 ± 12	233 ± 13
2 µg/kg	240 ± 8	252 ± 12	248 ± 23	240 ± 16	246 ± 19	254 ± 19	239 ± 13	236 ± 6	243 ± 8
5 µg/kg	251 ± 24	255 ± 26	255 ± 18	251 ± 19	257 ± 13	255 ± 12	255 ± 18	254 ± 10	263 ± 12

Values are mean ± s.d.

No significant change was observed in any group.

Table 4 Effects of 5IA on mean arterial blood pressure (% of baseline)

	Baseline	1 min	2 min	3 min	5 min	15 min	30 min	45 min	60 min
Vehicle	100	103 ± 2	105 ± 1	97 ± 6	91 ± 2	100 ± 5	104 ± 10	101 ± 11	100 ± 10
1 µg/kg	100	101 ± 6	106 ± 5	103 ± 11	104 ± 11	101 ± 14	103 ± 8	97 ± 4	94 ± 5
2 µg/kg	100	99 ± 2	99 ± 5	96 ± 16	99 ± 17	89 ± 11	94 ± 3	94 ± 7	91 ± 6
5 µg/kg	100	95 ± 3	94 ± 16	99 ± 11	102 ± 12	108 ± 8	99 ± 6	103 ± 5	112 ± 19

Values are mean ± s.d.

No significant change was observed in any group.

Table 5 Effects of 5IA on blood gas parameters

		Baseline	5 min	15 min	30 min	45 min	60 min
pH	Vehicle	7.43 ± 0.03	7.42 ± 0.03	7.42 ± 0.03	7.43 ± 0.02	7.42 ± 0.02	7.41 ± 0.01
	1 µg/kg	7.37 ± 0.03	7.37 ± 0.03	7.36 ± 0.02	7.37 ± 0.02	7.37 ± 0.02	7.36 ± 0.04
	2 µg/kg	7.37 ± 0.02	7.35 ± 0.02	7.36 ± 0.02	7.35 ± 0.03	7.35 ± 0.03	7.36 ± 0.04
	5 µg/kg	7.39 ± 0.06	7.36 ± 0.05	7.37 ± 0.04	7.37 ± 0.04	7.38 ± 0.03	7.38 ± 0.04
PCO ₂ (mmHg)	Vehicle	48.0 ± 6.7	48.4 ± 6.1	49.0 ± 7.0	45.7 ± 2.6	44.9 ± 1.8	45.1 ± 1.5
	1 µg/kg	44.8 ± 1.9	44.3 ± 3.2	46.3 ± 2.0	45.6 ± 1.8	44.9 ± 3.7	44.1 ± 2.9
	2 µg/kg	50.4 ± 5.7	53.5 ± 9.9	48.9 ± 3.6	46.6 ± 3.7	44.5 ± 4.4	43.6 ± 6.4*
	5 µg/kg	48.0 ± 3.3	50.0 ± 2.7	48.4 ± 3.5	45.8 ± 2.8	44.9 ± 1.4	43.7 ± 2.0
PO ₂ (mmHg)	Vehicle	74.6 ± 5.1	75.0 ± 2.4	76.4 ± 4.6	75.4 ± 5.0	77.9 ± 5.5	79.0 ± 3.3
	1 µg/kg	80.5 ± 6.5	78.4 ± 8.7	80.3 ± 8.4	80.8 ± 7.3	80.2 ± 7.9	78.9 ± 5.9
	2 µg/kg	77.9 ± 9.2	72.2 ± 2.5	76.1 ± 4.2	81.3 ± 4.3	80.3 ± 9.8	83.0 ± 5.9
	5 µg/kg	75.8 ± 6.9	71.2 ± 9.3	76.3 ± 4.5	79.0 ± 3.6	79.6 ± 2.8	83.7 ± 0.3*

Values are mean ± s.d. *p < 0.05 vs. Baseline.

Brain SPECT

Brain SPECT was performed at 4 hr after the administration of 171 MBq of [¹²³I]5IA. The subject received Lugol's solution (containing 400 mg of potassium iodide) orally 30 min prior to receiving [¹²³I]5IA. SPECT images were acquired for 20 min with a three-headed rotating gamma camera system (PRISM 3000, Picker International, Inc., USA) equipped with low-energy, high resolution, fanbeam collimators. This system provided a spatial resolution of 8.0 mm full-width at half-maximum (FWHM) at the center of the field of view with a sensitivity of 135 cps/MBq.

All SPECT images were filtered with a Butterworth filter (cutoff frequency, 0.25; order, 4) and reconstructed using a filtered backprojection algorithm with a ramp filter. Attenuation correction was performed using the ellipses outer line approximation and Chang's method (coefficient of 0.06/cm), which assumes that the attenuation process is homogeneous throughout the brain and can be described by an exponential function.

RESULTS

Behavior

In all three dose groups tested (0.1 μg/kg, 1 μg/kg, and 10 μg/kg), no changes were observed in the righting reflex or motor functions such as grip, walking and tonus of muscle in mice after administration of 5IA. No changes in spontaneous locomotion or grooming were noted in the animals administered 1 μg/kg of 5IA or less. In the 10 μg/kg treated group, decreases in spontaneous locomotion (5 mice in 5 mice) and grooming (2 mice in 5 mice) were observed 0–30 min after 5IA administration, but this sedative effect was transient and disappeared within 30 min post-administration (Table 1).

No significant difference was observed in body weight among control or 5IA-treated groups at 7 days after drug administration. This suggests that at 10 μg/kg or less, 5IA has no sub-acute toxicity (Fig. 1).

Physiological parameters

The administration of 5 μg/kg of 5IA immediately resulted in a significant increase in the respiratory rate (111 ± 4 breaths/min at baseline and 162 ± 12 breaths/min at 1 min), and this increase was significant until 45 min (128 ± 6 breaths/min at 45 min). The administration of 2 μg/kg also tended to increase the respiratory rate, although not significantly (111 ± 7 at baseline, 119 ± 16 at 1 min and 131 ± 15 at 15 min). On the other hand, no significant changes were noted in the group treated with vehicle or 1 μg/kg of 5IA (Table 2). Heart rate averaged 236 ± 16 beats/min in the vehicle-treated group with no significant difference from the values for the three groups treated with 5IA (Table 3). In rats administered a dose of 5 μg/kg or less, 5IA did not produce any changes in mean arterial blood pressure (MABP) (74 ± 12 mmHg at basal and

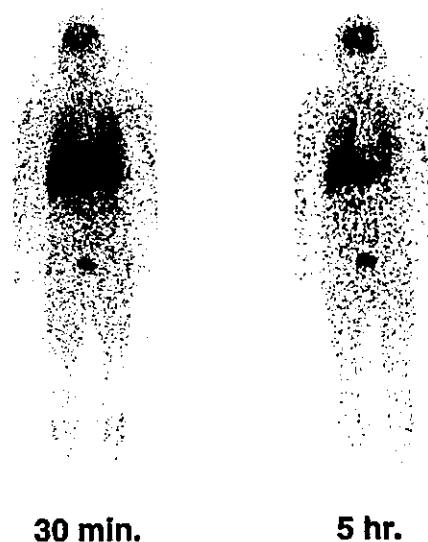


Fig. 2 Typical anterior whole-body images 30 min and 5 hr after the intravenous administration of [¹²³I]5IA. Brain, lungs, liver and bladder were clearly visualized in both images.

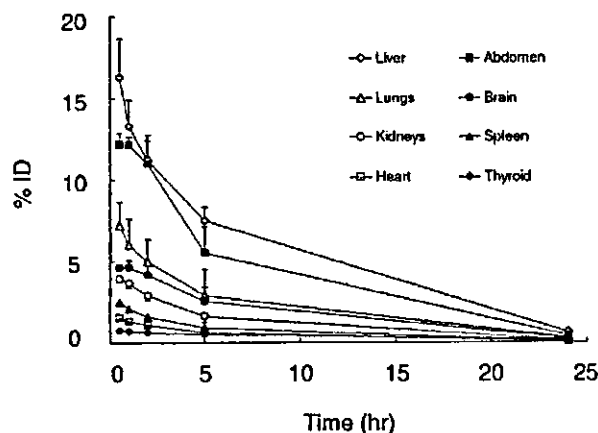


Fig. 3 Time-activity curves for various organs. Data were not corrected for decay and are expressed as percent injected radioactivity of [¹²³I]5IA. Each point represents the mean ± s.d. for all subjects.

Table 6 Mean residence times for all subjects

	Residence time (hr)
Liver	1.36 ± 0.15
Urinary bladder content	1.24 ± 0.30
Upper large intestine	0.79 ± 0.04
Lower large intestine	0.64 ± 0.03
Lungs	0.56 ± 0.28
Brain	0.47 ± 0.14
Small intestine	0.41 ± 0.02
Kidneys	0.31 ± 0.06
Spleen	0.18 ± 0.01
Thyroid	0.14 ± 0.06
Rest of body	4.57 ± 1.29

Values are the mean ± s.d.

91–105%, 94–106%, 89–100%, and 94–112% of baseline during 60 min after administration of vehicle, 1 $\mu\text{g}/\text{kg}$, 2 $\mu\text{g}/\text{kg}$, and 5 $\mu\text{g}/\text{kg}$, respectively) (Table 4). Rats administered 100 $\mu\text{g}/\text{kg}$ of 5IA showed transient increases in both heart rate and MABP.

No changes in blood pH or blood gases were noted in the animals administered 1 $\mu\text{g}/\text{kg}$ of 5IA. In rats administered 2 $\mu\text{g}/\text{kg}$ and 5 $\mu\text{g}/\text{kg}$ of 5IA, PCO_2 tended to decrease and PO_2 tended to increase at 60 min after injection (Table 5).

Biodistribution

Serial whole-body images of [^{123}I]5IA are shown in Figure 2. The temporal distribution profiles of the radioactivity in various organs are shown in Figure 3. At 30 min after injection, high levels of radioactivity were accumulated in the liver and urinary bladder, and moderate levels in the lungs, kidneys and brain. The radioactivity in the liver and lungs was rapidly eliminated. Penetration of the blood-brain barrier peaked at 1 hr after administration and was followed by a gradual decrease. The radioactivity in the kidneys decreased gradually with time. A small amount of radioactivity was observed in the thyroid. Twenty-four hours after injection, less than 1% of the injected radioactivity remained in any organs. The biological half-life of [^{123}I]5IA averaged 7.2 ± 4.0 hr.

The radioactivity in the urinary bladder increased rapidly, indicating prompt excretion through the renal system. The mean measured urinary excretion 24 hr after injection was $74 \pm 4\%$. No clear evidence of biliary excretion was seen on the images. Furthermore, the administration of [^{123}I]5IA did not cause any changes in blood, liver, or urine parameters.

Table 7 Radiation dose estimates for [^{123}I]5IA

Target organ	Absorbed dose ($\mu\text{Gy}/\text{MBq}$)
Thyroid	145 \pm 61
Urinary bladder wall	98 \pm 21
Lower large intestine wall	63 \pm 2.7
Upper large intestine wall	54 \pm 2.3
Kidneys	35 \pm 5.8
Spleen	32 \pm 2.3
Liver	32 \pm 2.9
Small intestine	25 \pm 1.2
Lungs	18 \pm 7.4
Ovaries	18 \pm 0.9
Uterus	17 \pm 0.8
Gallbladder wall	15 \pm 1.2
Heart wall	15 \pm 3.7
Brain	14 \pm 4.2
Bone surfaces	11 \pm 2.2
Pancreas	10 \pm 1.5
Adrenals	10 \pm 1.6
Total body	8.6 \pm 1.2
Stomach	8.6 \pm 1.4
Red marrow	6.9 \pm 1.1
Muscle	6.7 \pm 1.0
Testes	6.3 \pm 0.6
Thymus	5.6 \pm 1.6
Breasts	4.3 \pm 1.2
Skin	3.8 \pm 0.8
Effective dose equivalent*	30 \pm 1.4
Effective dose*	32 \pm 2.6

Values are the mean \pm s.d. *Units are $\mu\text{Sv}/\text{MBq}$.

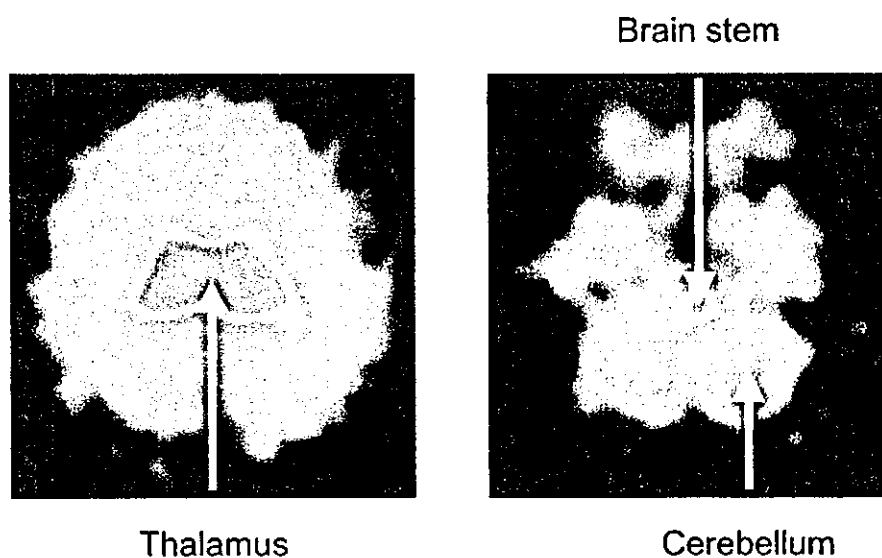


Fig. 4 SPECT images acquired 4 hr after administration of [^{123}I]5IA. The distribution of [^{123}I]5IA was associated with the known distribution of nAChR in human brain (thalamus > brain stem > cerebellum > cortex).

Dosimetry

Table 6 shows mean residence times for three subjects calculated from the time-activity curves. The residence times for urinary bladder content were calculated using the dynamic bladder model and those for the intestinal tracts, using the GI tract model. The dataset of each subject was fitted independently. The residence time was highest for the rest of body, followed by the liver and the urinary bladder. From these data and the biological half-lives of each subject, radiation absorbed doses were estimated using the MIRDOSE 3.1 software and the mean values obtained are shown in Table 7.

The highest radiation dose was to the thyroid, followed by the urinary bladder wall, lower large intestine wall and upper large intestine wall. The effective dose equivalent was $30 \pm 1 \mu\text{Sv/MBq}$.

Brain SPECT

The SPECT image obtained 4 hr after the administration of [^{123}I]5IA revealed the highest uptake of radioactivity to be in the thalamus. The radioactivity in the brain stem and the cerebellum was greater than that in the cerebral cortices (Fig. 4).

DISCUSSION

The safety of a radioligand is determined by both its toxicity and radiation.

Since the righting reflex remained unchanged and grip, walking and tonus of muscle were normal in mice administered $10 \mu\text{g/kg}$ of 5IA or less, 5IA had no effect on motor functions or static senses at $10 \mu\text{g/kg}$ or less. On the other hand, transient decreases in spontaneous locomotion were observed in all mice administered $10 \mu\text{g/kg}$ of 5IA. The inhibitory effect on the central nervous system seems to be responsible for this finding, since motor dysfunctions were not observed at this dose. Thus, since no abnormal behavior was observed at $1 \mu\text{g/kg}$ or less, the NOEL of 5IA was $1 \mu\text{g/kg}$.

The experiments on physiological parameters demonstrated that the respiratory rate tended to increase in rats injected with $2 \mu\text{g/kg}$ and $5 \mu\text{g/kg}$ of 5IA. Since nicotine has also been reported to increase the respiratory rate,¹⁸ the effect of 5IA on respiration may be mediated by nAChR. The respiratory rate, cardiovascular parameters and blood gas parameters were not changed from the baseline in the $1 \mu\text{g/kg}$ -treated group. Therefore, the experiments on physiological parameters also indicated that the NOEL was $1 \mu\text{g/kg}$. Given that an epibatidine analogue was lethal (30%) at an intravenous dose of $1.5 \mu\text{g/kg}$,¹⁹ 5IA has a greatly reduced toxicity profile. The lower toxicity of 5IA might be associated with its low affinity for the $\alpha 3\beta 4$ subtype, to which epibatidine binds with high affinity.^{20,21}

The specific radioactivity of [^{123}I]5IA is important to determine the chemical mass of 5IA to be administered. In

the present study, a very high specific radioactivity of more than $169 \text{ GBq}/\mu\text{mol}$ was obtained. Based on the uptake of [^{123}I]5IA by the brain, we estimated that 185 MBq of [^{123}I]5IA would be sufficient for SPECT imaging in humans. In this case, the chemical mass of [^{123}I]5IA corresponds to less than 5.3 ng/kg (18.2 pmol/kg) for a 60 kg individual (total dose; $0.32 \mu\text{g}$), which is about 190 times lower than the NOEL and about 230,000 times lower than the LD_{50} ($4.2 \mu\text{mol/kg}$).²² Thus, these results would support the utilization of [^{123}I]5IA in human nAChR imaging.

From the point of view of radiation protection, another factor determining the safety of a radioligand, the radiation dose of [^{123}I]5IA was estimated from whole-body images. Following injection of [^{123}I]5IA, the majority (~75%) of the radioactivity was excreted in urine 24 hr after administration, demonstrating that [^{123}I]5IA is mainly cleared from the renal system. The biological half-life of [^{123}I]5IA averaged 7.2 hr. Based on the biodistribution data, the effective dose equivalent was calculated to be $30 \mu\text{Sv/MBq}$. This value is in agreement with the results of another group²³ and lower than that of other ^{123}I -labeled receptor imaging ligands such as [^{123}I]IBF ($41 \mu\text{Sv/MBq}$)²⁴ and [^{123}I]iodo-PK 11195 ($40 \mu\text{Sv/MBq}$).²⁵ On the other hand, the administration of 171 MBq of [^{123}I]5IA ($0.0049 \mu\text{g/kg}$) clearly revealed a regional SPECT image which is consistent with the distribution of nAChR in human brain²; that is, the level of radioactivity was highest in the thalamus, high in the brain stem, moderate in the cerebellum and low in the cortical area. So, even if 185 MBq of [^{123}I]5IA is administered, the effective dose equivalent is estimated to be 5.6 mSv , which is almost the same as the average effective dose equivalent per patient from nuclear medicine (5 mSv).²⁶ Thus, the use of up to 185 MBq of [^{123}I]5IA may be adequate for SPECT imaging of nAChR in humans.

The highest absorbed dose was estimated in the thyroid based on whole-body imaging. This result indicates the necessity for thyroid blockade by the administration of Lugol's solution before the use of [^{123}I]5IA.

In conclusion, the NOEL of 5IA was $1 \mu\text{g/kg}$ and therefore, it is predicted that [^{123}I]5IA injected at the usual clinical dose would have no pharmacological effect. In addition, the radiation absorbed dose estimated based on the results of whole-body imaging appeared acceptable for clinical SPECT imaging. Furthermore, the regional distribution of radioactivity in the image of human brain was associated with the known nAChR distribution. These results highlight the promise of [^{123}I]5IA as a ligand for the SPECT imaging of nAChR in humans.

ACKNOWLEDGMENTS

This work was supported in part by a grant-in-aid for Scientific Research from the Ministry of Education, Science and Technology of Japan, a grant from 21st Century COE program

"Knowledge Information Infrastructure for Genome Science" and a grant from the Smoking Research Foundation. The authors thank Nihon Medi-Physics Co. Ltd. for providing sodium [¹²³I]iodine.

REFERENCES

- Gotti C, Fornasari D, Clementi F. Human neuronal nicotinic receptors. *Prog Neurobiol* 1997; 53: 199–237.
- Paterson D, Nordberg A. Neuronal nicotinic receptors in the human brain. *Prog Neurobiol* 2000; 61: 75–111.
- Akaike A, Tamura Y, Yokota T, Shimohama S, Kimura J. Nicotine-induced protection of cultured cortical neurons against *N*-methyl-D-aspartate receptor-mediated glutamate cytotoxicity. *Brain Res* 1994; 644: 181–187.
- Holladay MW, Bai H, Li Y, Lin NH, Daanen JF, Ryther KB, et al. Structure-activity studies related to ABT-594, a potent nonopioid analgesic agent: effect of pyridine and azetidine ring substitutions on nicotinic acetylcholine receptor binding affinity and analgesic activity in mice. *Bioorg Med Chem Lett* 1998; 8: 2797–2802.
- Burghaus L, Schutz U, Krempel U, de Vos RA, Jansen Steur EN, Wevers A, et al. Quantitative assessment of nicotinic acetylcholine receptor proteins in the cerebral cortex of Alzheimer patients. *Brain Res Mol Brain Res* 2000; 76: 385–388.
- Shimohama S, Taniguchi T, Fujiwara M, Kameyama M. Changes in nicotinic and muscarinic cholinergic receptors in Alzheimer-type dementia. *J Neurochem* 1986; 46: 288–293.
- Burghaus L, Schutz U, Krempel U, Lindstrom J, Schroder H. Loss of nicotinic acetylcholine receptor subunits alpha4 and alpha7 in the cerebral cortex of Parkinson patients. *Parkinsonism Relat Disord* 2003; 9: 243–246.
- Guan ZZ, Nordberg A, Mousavi M, Rinne JO, Hellstrom-Lindahl E. Selective changes in the levels of nicotinic acetylcholine receptor protein and of corresponding mRNA species in the brains of patients with Parkinson's disease. *Brain Res* 2002; 956: 358–366.
- Chefer SI, Horti AG, Lee KS, Koren AO, Jones DW, Gorey JG, et al. *In vivo* imaging of brain nicotinic acetylcholine receptors with 5-[¹²³I]iodo-A-85380 using single photon emission computed tomography. *Life Sci* 1998; 63: PL355–360.
- Fujita M, Tamagnan G, Zoghbi SS, Al-Tikriti MS, Baldwin RM, Seibyl JP, et al. Measurement of alpha4beta2 nicotinic acetylcholine receptors with [¹²³I]5-I-A-85380 SPECT. *J Nucl Med* 2000; 41: 1552–1560.
- Musachio JL, Scheffel U, Finley PA, Zhan Y, Mochizuki T, Wagner HN Jr, et al. 5-[I-125/123]iodo-3(2(S)-azetidylmethoxy)pyridine, a radioiodinated analog of A-85380 for *in vivo* studies of central nicotinic acetylcholine receptors. *Life Sci* 1998; 62: PL351–357.
- Musachio JL, Villemagne VL, Scheffel UA, Dannals RF, Dogan AS, Yokoi F, et al. Synthesis of an I-123 analog of A-85380 and preliminary SPECT imaging of nicotinic receptors in baboon. *Nucl Med Biol* 1999; 26: 201–207.
- Saji H, Ogawa M, Ueda M, Iida Y, Magata Y, Tominaga A, et al. Evaluation of radioiodinated 5-iodo-3-(2(S)-azetidylmethoxy)pyridine as a ligand for SPECT investigations of brain nicotinic acetylcholine receptors. *Ann Nucl Med* 2002; 16: 189–200.
- United States Government. Single dose acute toxicity testing for pharmaceuticals. *Federal Register* 1996; 61: 43934–43935.
- Cloutier RJ, Smith SA, Watson EE, Snyder WS, Warner GG. Dose to the fetus from radionuclides in the bladder. *Health Phys* 1973; 25: 147–161.
- International Commission on Radiological Protection. *Limits for intakes of radionuclides by workers*. New York; Pergamon Press, 1979.
- Stabin MG. MIRDOSE: personal computer software for internal dose assessment in nuclear medicine. *J Nucl Med* 1996; 37: 538–546.
- Volle RL, Koelle GB. Ganglionic stimulating and blocking agents. In: *The Pharmacological Basis of Therapeutics*, Goodman LS, Gilman A (eds), New York; The Macmillan Company, 1970: 585–600.
- Molina PE, Ding YS, Carroll FI, Liang F, Volkow ND, Pappas N, et al. Fluoro-norchloroepibatidine: preclinical assessment of acute toxicity. *Nucl Med Biol* 1997; 24: 743–747.
- Stauderman KA, Mahaffy LS, Akong M, Velicelebi G, Chavez-Noriega LE, Crona JH, et al. Characterization of human recombinant neuronal nicotinic acetylcholine receptor subunit combinations alpha2beta4, alpha3beta4 and alpha4beta4 stably expressed in HEK293 cells. *J Pharmacol Exp Ther* 1998; 284: 777–789.
- Xiao Y, Meyer EL, Thompson JM, Surin A, Wroblewski J, Kellar KJ. Rat alpha3/beta4 subtype of neuronal nicotinic acetylcholine receptor stably expressed in a transfected cell line: pharmacology of ligand binding and function. *Mol Pharmacol* 1998; 54: 322–333.
- Silver W, Nordberg A, Langstrom B, Mukhin AG, Koren AO, Kimes AS, et al. Development of ligands for *in vivo* imaging of cerebral nicotinic receptors. *Behav Brain Res* 2000; 113: 143–157.
- Fujita M, Seibyl JP, Vaupel DB, Tamagnan G, Early M, Zoghbi SS, et al. Whole-body biodistribution, radiation absorbed dose, and brain SPET imaging with [¹²³I]5-I-A-85380 in healthy human subjects. *Eur J Nucl Med Mol Imaging* 2002; 29: 183–190.
- van Dyck CH, Seibyl JP, Stubbs JB, Zoghbi S, Wisniewski G, Baldwin RM, et al. Human biodistribution and dosimetry of the SPECT D₂ dopamine receptor radioligand [¹²³I]IBF. *Nucl Med Biol* 1996; 23: 9–16.
- Versijpt J, Dumont F, Thierens H, Jansen H, De Vos F, Slegers G, et al. Biodistribution and dosimetry of [¹²³I]iodo-PK 11195: a potential agent for SPET imaging of the peripheral benzodiazepine receptor. *Eur J Nucl Med* 2000; 27: 1326–1333.
- Beekhuis H. Population radiation absorbed dose from nuclear medicine procedures in The Netherlands. *Health Phys* 1988; 54: 287–291.